LBL-32712
UC-405
Preprint

Lawrence Berkeley Laboratory

UNIVERSITY OF CALIFORNIA

Physics Division

Mathematics Department

To be submitted for publication

Lagrangian Numerical Methods Which Preserve the Hamiltonian Structure of Incompressible Fluid Flow

T.F. Buttke

July 1992

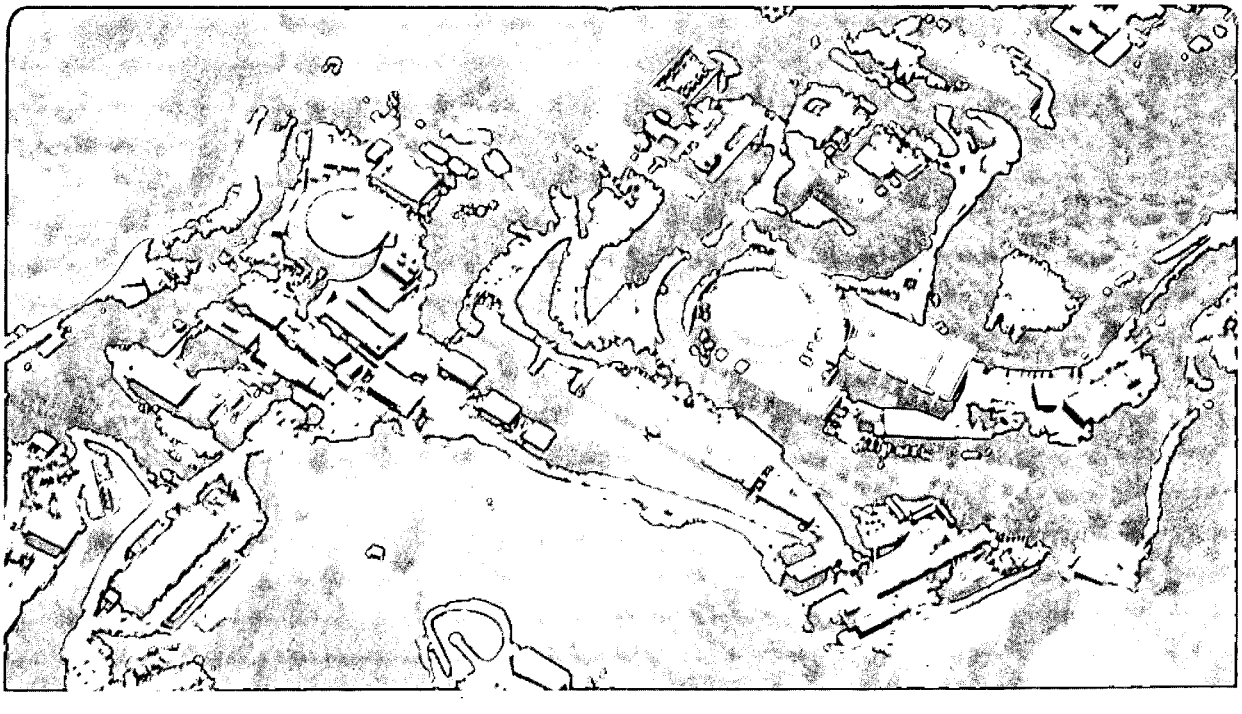

| LOAN COPY |
|Circulates |
|for 4 weeks| Bldg. 50 Library.
Copy 2
LBL-32712

Prepared for the U.S. Department of Energy under Contract Number DE-AC03-76SF00098

DISCLAIMER

This document was prepared as an account of work sponsored by the United States Government. While this document is believed to contain correct information, neither the United States Government nor any agency thereof, nor the Regents of the University of California, nor any of their employees, makes any warranty, express or implied, or assumes any legal responsibility for the accuracy, completeness, or usefulness of any information, apparatus, product, or process disclosed, or represents that its use would not infringe privately owned rights. Reference herein to any specific commercial product, process, or service by its trade name, trademark, manufacturer, or otherwise, does not necessarily constitute or imply its endorsement, recommendation, or favoring by the United States Government or any agency thereof, or the Regents of the University of California. The views and opinions of authors expressed herein do not necessarily state or reflect those of the United States Government or any agency thereof or the Regents of the University of California.

LBL-32712

LAGRANGIAN NUMERICAL METHODS WHICH PRESERVE THE HAMILTONIAN STRUCTURE OF INCOMPRESSIBLE FLUID FLOW[1]

Thomas F. Buttke

Courant Institute of Mathematical Sciences
New York University
New York, NY 10012
and
The Institute for Advanced Study
Olden Lane
Princeton, NJ 08540

July 1992

[1] This work was supported in part by the Applied Mathematical Sciences Subprogram of the Office of Energy Research, U.S. Department of Energy under Contract DE-AC03-76SF00098 while the author was visiting Lawrence Berkeley Laboratory, in part by the U.S. Department of Energy under Contract DEFG0288-ER25053, and in part by the National Science Foundation under Grant DMS-9100383.

Lagrangian Numerical Methods which Preserve the Hamiltonian Structure of Incompressible Fluid Flow

Thomas F. Buttke
Courant Institute of Mathematical Sciences
New York University
New York, NY 10012
and
The Institute for Advanced Study
Olden Lane
Princeton, NJ 08540

July 21, 1992

Abstract

We present a Lagrangian numerical method valid in any space dimension for approximating solutions to the Incompressible Euler Equation. The method is based on the canonical Hamiltonian formulation of incompressible flow. The method preserves at least three invariants of the flow: the kinetic energy, the impulse, and the angular momentum. We present numerical results which validate the method and elucidate the structure of the Hamiltonian variables in two and three dimensions.

1 Introduction

The description of the evolution of a system in terms of a Hamiltonian is the basis for the study of many physical systems. Once a system is described in terms of a Hamiltonian many properties of the system can be determined by the symmetries of the Hamiltonian. Oseledets [1] introduced a canonical Hamiltonian for the incompressible Euler equations in any number of space dimensions for the case where the fluid has a constant density. The work of Oseledets was based on the discrete Hamiltonian system introduced by Roberts [2] which asymptotically describes the evolution of vortex dipoles. In two dimensions the Hamiltonian structure introduced by Oseledets [1] is different from the point-vortex Hamiltonian structure introduced by Onsager [3].

In this paper we introduce two dimensional and three dimensional Lagrangian numerical methods based on the Hamiltonian formulation introduced by Oseledets. The numerical methods have several important properties which result from the fact that the methods are derived from an equation which has a Hamiltonian structure. The methods preserve the invariants: kinetic energy, impulse and angular momentum. Although we explicitly introduce the methods in two and three space dimensions, the numerical methods are valid in any number of dimensions and have the same basic properties.

The Hamiltonian structure of incompressible fluid flow is described in terms of a variable which we call the *velicity*. The velicity has units of velocity but satisfies an evolution equation which is similar to the evolution equation for the vorticity. If we make the analogy

between the magnetic field in magnetostatics [4] and the incompressible velocity field in fluid flow, the current density is analogous to the vorticity and the dipole density (magnetization) is analogous to the velicity; for this reason we denote the velicity by M.

2 Definition of the Velicity

Consider the incompressible Euler's equation

$$\frac{\partial u}{\partial t} + u \cdot \nabla u = -\frac{\nabla p}{\rho} \quad ,$$

where u is the velocity, $\nabla \cdot u = 0$, p is the pressure and ρ is the density; we shall assume the density $\rho = 1$ for most of the paper. In two and three dimensions we define the vorticity ω as

$$\omega \equiv \nabla \times u \quad ;$$

the equivalent extension to higher dimensions is to interpret u as a 1-form and $\omega \equiv du$ is the 2-form obtained by taking the differential of u [5]. The velicity M is then defined as any 1-form (vector field) such that $\omega = dM$ or in three dimensions such that $\omega = \nabla \times M$. Since $du = dM$ ($\nabla \times u = \nabla \times M$) we have that u and M are equivalent up to a gradient; that is

$$M = u + \nabla \phi \quad ,$$

where ϕ is a scalar function. This is commonly known as the Helmholtz or Hodge decomposition. The velocity u is uniquely determined from the velicity M by solving Poisson's equation

$$\Delta \phi = \nabla \cdot M$$

for ϕ to obtain $u = M - \nabla \Delta^{-1}\{\nabla \cdot M\}$; that is we solve Poisson's equation for ϕ and use $u = M - \nabla \phi$.

The evolution equation for M is given by

$$\frac{\partial M_i}{\partial t} + u \cdot \nabla M_i = -M_j \frac{\partial u_j}{\partial x_i} \quad , \tag{1}$$

where we have used the implied summation convention and the subscripts indicate the Cartesian components of the vectors; this equation can be motivated by considering the evolution of the impulse in a fluid [6] and the velicity can be interpreted as an impulse density. If we substitute $M_i = u_i + \partial_i \phi$ into eq (1) we obtain that

$$\frac{\partial u}{\partial t} + u \cdot \nabla u = -\nabla\{\frac{1}{2}u^2 + \frac{D\phi}{Dt}\} \quad ,$$

where $D/Dt \equiv \partial/\partial t + u \cdot \nabla$ is the substantial or material derivative. With the identification that $p = \{\frac{1}{2}u^2 + D\phi/Dt\}$, we see that eq (1) is equivalent to the incompressible Euler's equation.

The velicity is not unique; however, this proves to be useful since it is convenient to choose M differently for different circumstances. A possible choice for M initially is to take $M(x,0) = u(x,0)$; however, unless the flow is steady $M(x,t) \neq u(x,t)$ at later times.

For flows in unbounded domains it is convenient to choose the velicity so that it has compact support; if the vorticity is compact this can always be done (in two dimensions we must make the additional assumption that the flow has finite kinetic energy). We can show

this result via a simple construction. Assume that the support of the vorticity is inside of a ball of radius R centered at the origin. Outside of the ball the velocity can be written as $u = -\nabla\psi$ where $\Delta\psi = 0$, for some ψ. With this in mind we define a velicity M_c as

$$M_c \equiv u - \nabla \int_{\infty}^{r} (\hat{r} \cdot u) dr \quad , \tag{2}$$

where $\hat{r}$ is the unit vector in the radial direction. M_c is compact since outside of the ball of radius R, $M_c = 0$; we can show this by writing ψ as a sum of spherical harmonics (in whatever dimension we are considering). By taking the divergence of eq (2) we find that

$$\phi = -\int_{\infty}^{r} (\hat{r} \cdot u) dr \quad ,$$

we see that ψ, the potential part of the velocity field, is the same as the ϕ in the relation $M = u + \nabla\phi$. Thus we have shown that another candidate for the velicity M is obtained by subtracting off the potential part of the flow field.

If the velicity field is chosen initially to be compact it will remain compact for all later times; since from eq (1) velicity cannot be generated in the fluid. As is the case with the vorticity, the velicity can only be created at the boundaries of a fluid. In fact, generically, one can choose the velicity so that the support of the velicity coincides with the support of the vorticity. There are special cases, however, in which the support of the velicity must differ from the support of the vorticity; a symmetric jet or smoke ring for which the vorticity vanishes in the central region must have a nonzero velicity everywhere inside of the jet or smoke ring.

A simple argument shows that the velicity must be nonzero at the center of a jet or smoke ring. Consider the circulation $\Gamma \equiv \int_C u \cdot d\vec{l}$ in the fluid, where the integral is taken about a closed curve C. Now consider a curve C_0 which encircles a smoke ring but lies outside of the support of the vorticity, such that the circulation will have some nonzero value Γ_0. One can show that for an arbitrary closed curve C,

$$\int_C M \cdot d\vec{l} = \int_C u \cdot d\vec{l} \quad .$$

Consider calculating the circulation about C_0 using the velicity M instead of the velocity u; one would obtain that the circulation of the smoke ring is zero if we could pick the support of the velicity to coincide with the support of the vorticity in this case.

Having proven that the support of the velicity cannot coincide exactly with the support of the vorticity for all flows, we wish to argue that physically this is essentially what happens. Consider a sphere in an infinite fluid at rest initially, we can pick the velicity to be identically zero in this case. Let the fluid have a viscosity so that there will be vorticity generated at the surface of the sphere, but let the viscosity be small enough so that once the vorticity is generated there is essentially no diffusion of the vorticity. Now start accelerating the sphere through the fluid. The velicity and vorticity will be generated at the surface of the sphere; the vorticity and velicity both flow with the fluid velocity so that for all later times the support of the vorticity will coincide with the support of the velicity. This is the generic situation for unbounded flows and thus the support of the velicity will be as small as the support of the vorticity in real flow situations.

In the previous paragraph we considered the velicity in a viscous fluid, but eq (1) is valid only for Euler's equation; we now generalize eq (1) for the case of a viscous fluid. Let

the evolution of M be given by the equation:

$$\frac{\partial M_i}{\partial t} + u \cdot \nabla M_i = -M_j \frac{\partial u_j}{\partial x_i} + \nu \Delta M_i \quad . \tag{3}$$

By substituting $M_i = u_i + \partial_i \phi$, we can show that eq (3) is equivalent to the Navier-Stokes equation:

$$\frac{\partial u}{\partial t} + u \cdot \nabla u = -\nabla \{\frac{1}{2} u^2 + \frac{D\phi}{Dt} - \nu \Delta \phi\} + \nu \Delta u \quad .$$

We see that the pressure becomes $p = \{\frac{1}{2}u^2 + D\phi/Dt - \nu\Delta\phi\}$.

We now consider the inviscid equations again. Constant density incompressible fluid flows have many invariants. We wish to present some of those invariants in terms of the velicity.

The first invariant we consider is the impulse of the fluid [7]. The impulse I is defined in three dimensions as

$$I \equiv \frac{1}{2} \int_{R^3} r \times \omega \, dx \quad .$$

We substitute $\omega = \nabla \times M$ and integrate by parts, assuming M is compact, which follows if ω is, to find that

$$I = \frac{1}{2} \int_{R^3} r \times \omega \, dx = \int M dx \quad ; \quad .$$

this result also motivates describing the velicity as an impulse density. The generalization to any number of dimensions is to define the impulse as

$$I \equiv \int M dx \quad ; \tag{4}$$

one can show directly then from eq (1) that the impulse is an invariant the flow. This result is the motivation for describing the velicity as an *impulse density.*

The next invariant we consider is the kinetic energy. From the fact that $M = u + \nabla\phi$ and $\nabla \cdot u = 0$ and after an integration by parts we see that

$$\frac{1}{2} \int u^2 \, dx = \frac{1}{2} \int M \cdot u \, dx \quad . \tag{5}$$

We can show that this is an invariant directly from eq (1). We have that

$$\begin{aligned} \frac{d}{dt} \int \frac{1}{2} u^2 dx &= \int u \cdot \frac{\partial u}{\partial t} dx = \int u \cdot \frac{\partial M}{\partial t} dx \\ &= -\int_\Omega \partial_i (u_i u_j M_j) dx = -\int_{\partial\Omega} (\hat{n} \cdot u)(u \cdot M) da = 0 \quad , \end{aligned}$$

where we have assumed the usual boundary conditions $u \cdot \hat{n} = 0$ for an Eulerian flow and $\hat{n}$ is the outward normal to the domain under consideration.

The third invariant we consider is the angular momentum of the fluid [7]. The angular momentum Ω in three dimensions is defined as $\Omega \equiv \frac{1}{3} \int r \times (r \times \omega) d^3x$. Substitution of $\omega = \nabla \times M$ and integration by parts yields immediately

$$\Omega = \frac{1}{3} \int r \times (r \times \omega) d^3x = \int r \times M d^3x \quad . \tag{6}$$

The generalized invariant is defined as

$$\Omega \equiv \int (r \wedge M) \, dx \quad ,$$

which can be shown to be an invariant of the motion in any dimension directly from eq (1).

The final invariant we consider is the helicity. The helicity η is defined as $\eta \equiv \int(\omega \cdot u)dx$. An integration by parts yields immediately that $\eta = \int(\omega \cdot u)dx = \int(\omega \cdot M)dx$. Oseledets [1] noted that in three dimensions the *helicity density* is a scalar invariant when it is written in terms of the velicity. Using the vorticity equation $\partial\omega/\partial t + u \cdot \nabla\omega = \omega \cdot \nabla u$, and eq (1) we have immediately that

$$\frac{D(\omega \cdot M)}{Dt} = 0 \quad . \tag{7}$$

We can generalize eq (7) to any number of dimensions by noting that in three dimensions vortex lines evolve as material curves in the fluid [8]. Thus in order to generalize eq (7) we consider the evolution of a material curve. Let $x(\alpha, t)$ denote the usual flow map which gives the position x at time t of the fluid particle which was located at position α at time $t = 0$. The Jacobian J of the flow map is given by

$$J_{ij} = \frac{\partial x_j}{\partial \alpha_i} \quad .$$

Since $\partial x/\partial t = u$ we have immediately that

$$\frac{\partial J}{\partial t} = J \cdot \nabla u \quad ,$$

where $(J \cdot \nabla u)_{ij} = J_{ik}\partial_k u_j$ (using the implied summation convention). Thus we obtain the important generalization of eq (7) that

$$\frac{D(J \cdot M)}{Dt} = 0 \quad , \tag{8}$$

where $(J \cdot M)_i = M_j \partial x_j/\partial \alpha_i$. Thus we immediately obtain a solution for M in Lagrangian coordinates in terms of the Jacobian of the flow map:

$$M(\alpha, t) = J^{-1}(\alpha, t)J(\alpha, 0)M(\alpha, 0) \quad , \tag{9}$$

where we have not assumed that the Jacobian at $t = 0$ is the identity. The inverse in eq (9) exists for all times as long as it does initially since the flow is incompressible and therefore $\partial \mid J \mid /\partial t = 0$ [8], where $\mid J \mid$ denotes the determinant of J. In three dimensions the evolution of the velicity eq (9), is in a sense the inverse of the evolution of the vorticity, where

$$\omega(\alpha, t) = J(\alpha, t)J^{-1}(\alpha, 0)\omega(\alpha, 0) \quad .$$

Equation (8) also has an interesting physical interpretation. If we consider a parametrization such that initially the velicity is perpendicular to the surfaces $\alpha_1 =$ constant, eq (8) shows that the surfaces evolve so as to remain perpendicular to the velicity. We use eq (8) in presenting our numerical results in two dimensions by showing the evolution of the surfaces $dx \cdot M = 0$; see figs (1-10).

The numerical work presented here deals with constant density flows, however, before we conclude this section on background material for the velicity variable we wish to extend eq (1) to variable density flows. Variable density flows do not have the Hamiltonian structure introduced by Oseledets, however, the formulation of incompressible fluid mechanics in terms of the velicity is extremely useful and so we include the variable density equations here for completeness.

In order to derive an equation to describe the evolution of the velicity for variable density incompressible flows we follow the derivation of energy conservation following eq (5). Since kinetic energy is also conserved in variable density flows, the correct equation describing the evolution of the velicity should be identical to eq (1) with the addition of a term to account for the fact that gradients in the density generate vorticity in an incompressible flow. Also the Helmholtz decomposition must be modified appropriately. For variable density flows we relate the velicity M to the velocity u linearly as follows:

$$M = u + \frac{\nabla\phi}{\rho} \quad . \tag{10}$$

We substitute eq (10) into eq (1) and require that the resultant equation have the form of the variable density Euler's equation. As expected we find we must add a term to eq (1) so that the resultant equation has the desired form. We find that M must satisfy

$$\frac{\partial M_i}{\partial t} + u \cdot \nabla M_i = -M_j \frac{\partial u_j}{\partial x_i} - \frac{1}{2} u^2 \frac{\partial \ln \rho}{\partial x_i} \quad . \tag{11}$$

Substitution of eq (10) into eq (11) yields

$$\frac{\partial u}{\partial t} + u \cdot \nabla u = -\frac{\nabla\{\frac{1}{2}\rho u^2 + D\phi/Dt\}}{\rho} \quad , \tag{12}$$

where we have used the continuity equation $D\rho/Dt = 0$. Thus we see for the general variable density case the pressure of the fluid is given by

$$p = \{\frac{1}{2}\rho u^2 + \frac{D\phi}{Dt}\} \quad ,$$

where now ϕ is defined by eq (10). Energy conservation now follows from eqs (10,11) and the continuity equation:

$$\begin{aligned}
\frac{d}{dt}\int \frac{1}{2}\rho u^2 dx &= \int \frac{1}{2} u^2 \frac{\partial \rho}{\partial t} dx + \int \rho u \cdot \frac{\partial u}{\partial t} dx \\
&= -\int \frac{1}{2} u^2 (u \cdot \nabla \rho)\, dx + \int \rho u \cdot \frac{\partial M}{\partial t}\, dx - \int \rho u \cdot \frac{\partial(\nabla\phi/\rho)}{\partial t}\, dx \\
&= -\int u^2 (u \cdot \nabla \rho)\, dx - \int \rho u \cdot \nabla(u \cdot M)\, dx - \int \{u \cdot (M - u)\}(u \cdot \nabla \rho)\, dx \\
&= -\int_\Omega \partial_i(\rho u_i u_j M_j)\, dx = -\int_{\partial\Omega} \rho(\hat{n} \cdot u)(u \cdot M)\, da = 0 \quad ,
\end{aligned}$$

where once again we assume $u \cdot \hat{n} = 0$ as the boundary condition for Euler's equation.

3 The Lagrangian Numerical Method

In this section we present the Lagrangian numerical methods which are valid in any number of dimensions for constant density incompressible fluid flows. We shall try to make the presentation independent of the dimension of the space. The methods are based upon a discretization of eq (1). The methods preserve three invariants of incompressible fluid flow: kinetic energy, impulse, and angular momentum. In this paper we assume the fluid is in a unbounded domain. We shall deal with bounded domains in a future paper. The discretization is based on the discretization introduced and refined in [9, 10, 11, 12, 13].

We wish to approximate the velicity field $M(x,t)$ which evolves according to eq (1) with initial conditions $M(x,0)$; we denote our approximation to M as $\tilde{M}$. Given $\tilde{M}(x,t)$ we associate the incompressible velocity field $\tilde{u}(x,t)$ which is our approximation to $u(x,t)$ and is related to $\tilde{M}$ via the Helmholtz decomposition $\tilde{M} = \tilde{u} + \nabla\phi$. We define an approximation to $M(x,0)$ and then evolve the approximation according to eq (1).

We first define a mollification (blob) function f_δ as

$$f_\delta(x) = \frac{1}{\delta^d} f_0(x/\delta) \quad ,$$

where f_0 is a smooth function which has unit mass $\int f_0 dx = 1$, and whose first $p-1$ moments vanish

$$\int x^\alpha f_0 dx = 0, \quad \text{for} \quad 0 < |\alpha| \leq p-1 \quad ,$$

where α is the multi-index $x^\alpha \equiv x_{i_1}^{\alpha_1} x_{i_2}^{\alpha_2} \cdots x_{i_d}^{\alpha_d}$ and d is the space dimension. We define our initial approximation to M as follows:

$$\tilde{M}(x,0) = \sum_{i=1}^{N} f_\delta(x - x_i) m_i \quad , \tag{13}$$

where the x_i are equally spaced points on a regular mesh of spacing h, and $m_i \equiv h^d M(x_i, 0)$; points on an irregular mesh can be discretized appropriately, but for clarity we assume a regular mesh. The sum in eq (13) is over all points such that $M(x_i, 0) \neq 0$. The convergence properties are given in [13] and the approximation in eq (13) converges with order p as $h \to 0$ provided $h = \delta^\beta$, where $\beta < 1$. The approximation to M at later times is defined by defining evolution equations for the x_i and m_i and defining $\tilde{M}(x,t)$ as:

$$\tilde{M}(x,t) = \sum_{i=1}^{N} f_\delta(x - x_i(t)) m_i(t) \quad , \tag{14}$$

where the x_i satisfy

$$\frac{dx_i}{dt} = \tilde{u}(x_i) \quad , \tag{15}$$

and the m_i satisfy

$$\frac{d(m_i)_k}{dt} = -(m_i)_j \frac{\partial \tilde{u}_j(x_i)}{\partial (x_i)_k} \quad , \tag{16}$$

where the notation $(m_i)_k$ denotes the k-th component of the vector m_i and likewise for x_i; the notation is somewhat complicated but the right hand side of eq (16) is the same as appears in eq (1). The velocity $\tilde{u}$ is defined by

$$\tilde{u} = \tilde{M} - \nabla\phi \quad , \tag{17}$$

and the fact that $\nabla \cdot \tilde{u} = 0$; we note that $\tilde{u}$ is spatially as smooth as is f_δ. We expect that $\tilde{M} \to M$ as $h \to 0$ and therefore also $\tilde{u} \to u$, as is proven for vortex methods in [11, 12, 13]; our numerical results indicate that this is indeed the case.

We now construct $\tilde{u}$ explicitly and prove the invariance of the kinetic energy, impulse and angular momentum of the numerical scheme. One can show that

$$\tilde{u}(x) = \sum_{j=1}^{N} \{ m_j f_\delta(x - x_j) - (m_j \cdot \nabla)\nabla\psi(x - x_j) \} \quad , \tag{18}$$

where ψ satisfies $\Delta\psi = f_\delta$; for simplicity we assume that f_δ is radially symmetric. Outside of the support of f_δ eq (18) gives a dipole field for the velocity induced by a single blob of velicity. We define the discrete kinetic energy H of the method as an approximation to the kinetic energy $1/2 \int (M \cdot u)\, dx$;

$$\begin{aligned} H &\equiv \frac{1}{2}\sum_{k=1}^{N} m_k \cdot \tilde{u}(x_k) \\ &= \frac{1}{2}\sum_{j=1}^{N}\sum_{k=1}^{N} \{(m_j \cdot m_k) f_\delta(x_j - x_k) + (m_j \cdot \nabla_j)(m_k \cdot \nabla_k)\psi(x_j - x_k)\} \quad , \end{aligned} \tag{19}$$

where ∇_k indicates the gradient with respect to the x_k. In order to obtain the second equality in eq (19) we substituted eq (18) and used the fact that $\nabla_k \psi(x_j - x_k) = -\nabla_j \psi(x_j - x_k)$. We note that the discrete kinetic energy is finite because f_δ is a smooth function; this is in contrast to the singular form one obtains from Roberts' original work [2]. One can obtain the self-energy of a blob by evaluating the velocity at the origin for a single blob which is also located at the origin. One finds that the self-velocity u_0 of the blob located at x_k is

$$u_0 = \frac{d-1}{d} m_k f_\delta(0) = \frac{h^d}{\delta^d}\frac{d-1}{d} M_k f_0(0) \quad , \tag{20}$$

where d is the space dimension. Thus we see that in the limit $h \to 0$ with $h = \delta^\beta$ the self-velocity of a blob vanishes; for nonzero h and δ, however, $u_0 \neq 0$; the self-energy then is

$$\rho \frac{h^{2d}}{\delta^d}\frac{d-1}{2d} M_k^2 f_0(0) \quad ,$$

where we have included ρ the density of the fluid to make the self-energy dimensionally correct.

The discrete system can be written as a Hamiltonian system if we observe that

$$\frac{dx_k}{dt} = \nabla_{m_k} H \quad , \tag{21}$$

and

$$\frac{dm_k}{dt} = -\nabla_{x_k} H \quad , \tag{22}$$

where $\nabla_{m_k} H$ and $\nabla_{x_k} H$ indicate taking gradients with respect to the variables m_k and x_k. By a direct computation eq (15) is identical to eq (21) and eq (16) is identical to eq (22).

The preservation of the discrete invariants is an immediate consequence of the Hamiltonian structure of the system where H is identified as the Hamiltonian. The discrete kinetic energy is an invariant since $dH/dt = 0$ if the Hamiltonian does not explicitly depend on time [14]. Since the Hamiltonian is translation invariant we have that

$$I \equiv \sum_{i=1}^{N} m_i \quad , \tag{23}$$

is a constant of motion; we see that eq (23) is an approximation to the impulse $\int M\, dx$. The third invariant Ω is an approximation to the angular momentum $\int x \wedge M\, dx$,

$$\Omega \equiv \sum_{i=1}^{N} x_i \wedge m_i \quad , \tag{24}$$

and it is an invariant because the Hamiltonian is rotationally invariant. The fact that I and Ω are discrete invariants of motion can also be verified directly by calculating $[I, H] = 0$ and $[\Omega, H] = 0$ where I and Ω are defined by eqs (23,24) and $[\cdot,\cdot]$ denotes the Poisson bracket [14].

It is interesting to note that this finite particle system describing incompressible fluid flow has the same invariants as N bodies interacting via a central force such as gravity. In particular the asymptotic motion of two velicity particles colliding is completely determined by the three invariants H, I and Ω. This observation and the Hamiltonian structure make an alternative description of incompressible superfluid Helium possible; we will address this in future work.

4 Numerical Results

In this section we present some numerical results obtained using the approximation described in the previous section. We present results in both two and three dimensions. The results presented here are only meant to demonstrate the basic properties of the method and to validate it. In particular we do not advocate that the two dimensional method is better or worse than other two dimensional Lagrangian methods; however, we wish to emphasize the fact that the methods are formally the same independent of dimension. Therefore once the method is developed in two dimensions it is simple to extend the method to any number of dimensions. In the work presented here we developed the three dimensional method first and modified it for two dimensions. In future work, however, which will include boundaries and viscosity, it will be much simpler to develop the method in two dimensions where visualization is easier and then extend the method to three dimensions. The fact that the structure of the vorticity equations changes in going from two to three dimensions has made the development of three dimensional Lagrangian vorticity methods difficult.

The numerical method has several unique features as a Lagrangian method besides the obvious feature it shares with other methods; the fact that it produces a smooth velocity field $\tilde{u}$ which is exactly divergence-free at every time. The first important feature is that the vorticity $\nabla \times \tilde{u}$ is compact. Although this can be done for many methods in two dimensions, it is not possible to produce a compact vorticity field in three dimensions when the vorticity is used as the computational variable [6]. Another important feature of the method is the fact that discrete energy, impulse and angular momentum invariants are preserved. We observe that the preservation of these invariants causes the numerical method to preserve many of the important physical symmetries which are present in Eulerian flows; flows do not become unphysical because of numerical discretization artifacts.

For the three dimensional calculations presented here we used the following blob function:

$$f_0(x) = \frac{21}{31\pi} \begin{cases} 1, & \text{if } r \leq 1/2; \\ 1 - 10(r-1/2)^3 + 15(r-1/2)^4 - 6(r-1/2)^5, & \text{if } 1/2 < r \leq 3/2; \\ 0, & \text{if } r > 3/2, \end{cases}$$

where $r = |x|$. For the two dimensional calculations we used

$$f_0(x) = \frac{7}{2\pi} \begin{cases} 1 - 10r^3 + 15r^4 - 6r^5, & \text{if } r \leq 1; \\ 0, & \text{if } r > 1, \end{cases}$$

where again $r = |x|$. Both of the blob functions have continuous second derivatives. There is no particular reason for choosing the more complicated form for the three dimensional

blob function; choosing a form similar to the two dimensional case should work just as well and the formulas would be slightly shorter. The spatial derivative which must be calculated in eq (16) was evaluated exactly via eq (18). The velocity was also evaluated exactly via eq (18) using a direct summation technique. The equations of motion eqs (15,16) were solved exactly using fourth order Runge-Kutta. The error in solving the equations of motion was monitored by calculating the invariants H, I and Ω. Since the kinetic energy H is positive definite, it proves to be the most sensitive measure of error in integrating the system and we choose our time step so as to preserve the kinetic energy invariant to an accuracy of 1×10^{-7}. The impulse invariant and angular momentum invariant were constant to machine accuracy (1×10^{-15}) due to the exact algebraic cancellation of those invariants.

There are many things which can be done to improve the computational efficiency of the method, such as using a fast summation method [15, 16] to calculate the velocity, or introducing an approximation to calculate the spatial derivatives; however, in this paper we deliberately avoid any such approximations so that the basic method can be validated without the added complication of other numerical approximations. These improvements to the method will be addressed in future work.

In the two dimensional calculations, see figs (1-10), we present the results by showing the evolution of the surfaces which are perpendicular to M initially and remain perpendicular to M for all later times, as given by eq (8). We choose for the initial conditions a velicity field which points in the y-direction and thus the surfaces in two dimensions are lines of constant y value; see figs (1,5). In figs (1-10) these surfaces are drawn by simply connecting the locations of the velicity particles which are originally on the same surface. The circles in figs (1,5) are additional Lagrangian markers chosen to help show the evolution of the fluid and to emphasize the fact that the initial velicity magnitudes are chosen radially symmetric, as is discussed below.

The initial conditions for the two dimensional calculations, $M(x,0)$, is chosen to be a smooth dipole given in velicity variables as

$$M_2(x,0) = \begin{cases} 1 - 10r^3 + 15r^4 - 6r^5, & \text{if } r \leq 1; \\ 0, & \text{if } r > 1, \end{cases} \tag{25}$$

where $r = |x|$, and $M_1(x,0) = 0$. This produces an initial velocity which is given by eq (18) for a single particle. From eq (20) we see that the velocity of the point at the origin should be 1/2, at least initially; from fig (1) and fig (2) this is seen to be the case, although the velocity of the curve bounding the support of the velicity is considerably slower.

In figs (1-4) we show the results of approximating eq (25) with an initial grid with a spacing $h = 0.05$. This results in approximating eq (25) with 1245 points evenly spaced initially. We choose the smoothing parameter $\delta = 0.4$. In fig (3) we plot the direction of the velicity vectors m_i at their locations. We see that indeed the approximate velicity field evolves so as to remain perpendicular to the surface on which it was perpendicular initially.

In figs (5-10) we show the results of approximating the same initial conditions, eq (25), with a grid spacing $h = 0.025$ and leaving $\delta = 0.4$. This results in 5013 particles approximating the flow. In figs (5-9) we plot half of the surfaces $J \cdot M = 0$ and in fig (10) we plot a third of the surfaces. In comparing figs (1-4) with figs (5-10) we see that the results have converged to the limiting value as $h \to 0$. Because of the large number of points necessary to perform the calculations it is not possible to show the convergence as $\delta \to 0$ as accurately except for extremely short times.

In figs (11-16) we show the results of some generic three dimensional calculations. The lines shown in figs (11-16) are actual vortex lines of the continuous velocity field $\tilde{u}$. For

instance in fig (11) a Lagrangian curve C, initially a circle, is evolved with the fluid velocity $\tilde{u}$. At any desired time the vortex lines through C are calculated by numerically integrating the vorticity field $\nabla \times \tilde{u}$. Although there is no a priori numerical constraint which guarantees that the vortex lines which close initially will close at later times, we see that the approximation preserves this property in figs (11,12). No swirl is numerically introduced.

The initial conditions for the calculations shown in figs (11-12) are those which produce a vortex ring of large radius $R = 1$, with constant vorticity inside the torus of small radius $a = 0.4$. We choose the velicity so that it initially has only a z component, which is given by

$$M_3(x,0) = \begin{cases} (1+\sqrt{a^2-z^2}-r)/2a, & \text{if } (r-1)^2+z^2 \le a^2; \\ \sqrt{a^2-z^2}/a, & \text{if } z^2 \le a^2 \text{ and } r \le 1-\sqrt{a^2-z^2}; \\ 0, & \text{elsewhere;} \end{cases} \tag{26}$$

where $r^2 = x^2+y^2$. The velicity is normalized so that $\mid M \mid = 1$ at the origin. We can verify that eq (26) produces the correct vorticity by taking the curl of the velicity; note that the velicity is continuous whereas the vorticity is discontinuous.

The initial velicity eq (26) is approximated by 5696 points on a grid which is uniform in cylindrical coordinates r,θ,z; the average spacing is $h = 0.1$ and $\delta = 0.4$. The vortex lines which are shown in figs (11,12) are those which intersect a circular curve of radius 0.2 initially. Since the chosen initial conditions are not a steady state solution the vortex ring must evolve. Conservation of impulse and angular momentum prevent the ring from stretching in the radial direction. The ring evolves by stretching in the z direction while maintaining its cylindrical symmetry (see fig (12)) and eventually forms a thin urn-like structure. There is no cylindrical symmetry assumed in the calculation once the initial conditions are chosen.

In figs (13,14) we show the evolution of a flow in which the velocity has compact support inside of a torus. We choose a smooth velocity such that the support lies inside of a torus of large radius $R = 1$ and small radius $a = 0.2$. We define a divergence-free velocity u in terms of toroidal coordinates ρ, θ, ϕ as

$$\begin{aligned} u_\theta &= r\chi^2 f(\rho\chi/a) \\ u_\rho &= \frac{-n\epsilon\chi\rho}{r}\cos(n\theta) f(\rho\chi/a) \\ u_\phi &= \frac{-n\epsilon\chi\rho^2}{r}\cos(n\theta)\sin\phi\left(2f(\rho\chi/a)+\frac{\chi\rho}{a}f'(\rho\chi/a)\right)+\Omega_0\rho^2 f(\rho\chi/a) \quad , \end{aligned} \tag{27}$$

where f is given by the right hand side of eq (25), $\chi = 1+\epsilon\sin(n\theta)$, $r^2 = x^2+y^2$, $\rho^2 = (r-1)^2+z^2$, n is an integer, and a, ϵ and Ω_0 are parameters. For the flow in figs (13,14) we choose $a = 0.2$, $\epsilon = 0.0$, and $\Omega_0 = 25.0$. We approximated the flow with 5807 points, $h = 0.05$ and $\delta = 0.4$. In this example we choose $M(x,0) = u(x,0)$ initially. Although the velocity does not have a compact support for later times the velicity does. In fig (13) we show a single vortex line; note that now the vortex lines do not close initially and therefore should not close at later times either. The vortex lines wrap around torii; a single vortex line eventually covering a particular torus. In fig (14) we show the evolution of the vortex line we showed initially in fig (13). Because of the complicated structure of the vorticity in this calculation it would be difficult to do a similar calculation with a vorticity based method.

In the calculation shown in figs (15,16) we again choose an initial velocity given by eq (27) with compact support and pick $M = u$ initially. The choice of parameters is $a = 0.2$,

$\epsilon = 0.25$, $n = 1$ and $\Omega_0 = 25.0$. The difference between the initial conditions in fig (15) and those in fig (13) is that in fig (15) we vary the small radius of the torus as a function of θ, the angle around the torus. Thus as we see in fig (13) the vortex lines now change their pitch and radius as they wrap around the toroidal surface. In fig (16) we show the evolution of the vortex line shown originally in fig (15). Once again we see that performing a similar calculation in vorticity variables would be difficult. We wish to emphasize that the three invariants: kinetic energy, impulse and angular momentum are discrete invariants of the calculations shown here.

5 Conclusions

We have presented a Lagrangian numerical method which approximates the incompressible Euler's equation in any number of space dimensions and preserves the three important invariants: kinetic energy, impulse and angular momentum. We have presented calculations which validate and show the convergence of the numerical method. Although the results shown here are only meant to validate the method, some of the advantages of basing the numerical method on the Hamiltonian formulation of incompressible flow is apparent from the complex structures we have been able to calculate in three dimensions. Work is under way to improve the Lagrangian algorithms so as to handle flows with boundaries and viscosity. We are adding other numerical approximations to increase the computational efficiency of the method. We have also developed a finite difference code based on the velicity formulation which has similar properties to the Lagrangian methods [17].

6 Acknowledgements

We acknowledge support from the Department of Energy under contract DEFG0288-ER25053 and under contract DEAC03-76SF00098 while the author was visiting Lawrence Berkeley Laboratory, and from the National Science Foundation under grant DMS-9100383.

References

[1] V. I. Oseledets, *On a new way of writing the Navier-Stokes equation: The Hamiltonian formalism*, Commun. Moscow Math. Society, (1988); translated in Russ. Math. Surveys 44, 210-211 (1989).

[2] P. H. Roberts, *A Hamiltonian theory for weakly interacting vortices*, Matematica **19** 169-179 (1972).

[3] L. Onsager, *Statistical hydrodynamics*, Nuovo Cimento, suppl. to vol. 6, 279-287 (1949).

[4] J. D. Jackson, *Classical Electrodynamics*, John Wiley & Sons, New York, 1975.

[5] M. Spivak, *Calculus on Manifolds*, W. A. Benjamin Inc., Menlo Park, California, 1965.

[6] T. F. Buttke, to appear in proceedings of international workshop on Vortex Flows and Related Numerical Methods, held June 15-20, 1992 in Grenoble, France.

[7] G. K. Batchelor, *Fluid Dynamics*, Cambridge University Press, New York, 1973.

[8] A. J. Chorin, J. E. Marsden, *A Mathematical Introduction to Fluid Mechanics*, Springer-Verlag, New York, 1979.

[9] A. J. Chorin, *Numerical study of slightly viscous flow*, J. Fluid Mech., **57** 785-796 (1973).

[10] A. J. Chorin, *The evolution of a turbulent vortex*, Comm. Math. Phys., **83** 517-535 (1982).

[11] O. H. Hald, *Convergence of vortex methods for Euler's equations, II*, SIAM J. Numer. Anal., **16** 726-755 (1979).

[12] J. T. Beale, A. Majda, *Vortex methods II: higher order accuracy in two and three dimensions*, Math. Comp., **39** 29-52 (1982b).

[13] C. Anderson, C. Greengard, *On vortex methods*, SIAM J. Numer. Anal., **22** 413-440 (1985).

[14] H. Goldstein, *Classical Mechanics*, Addison-Wesley, Menlo Park, California, 1950.

[15] L. Greengard, V. Rokhlin, *A fast algorithm for particle simulations*, J. Comp. Phys., **73** 325-348 (1987).

[16] T. F. Buttke, *Fast Vortex Methods in Three Dimensions*, Lectures in Applied Mathematics: volume 28. Editors: C. Anderson and C. Greengard, AMS 1991.

[17] T. F. Buttke, *A Finite Difference method based on the velicity formulation of incompressible flows*, in preparation.

7 Figure Captions

Figure 1. The Initial Material Surfaces. The material surfaces are shown which are orthogonal to the velicity field for a grid spacing of $h = 0.05$. Each surface is at the position of the initial discretization. The circles are additional Lagrangian markers inserted to aid in the visualization of the flow.

Figure 2. The Evolution of the Material Surfaces. The evolution of the material surfaces are shown, $h = 0.05$.

Figure 3. The Direction of the Velicity Field. The direction of the velicity field is shown, demonstrating that it evolves so as to stay perpendicular to the material surfaces.

Figure 4. The Evolution of the Material Surfaces. The further evolution of the material surfaces are shown for $h = 0.05$.

Figure 5. The Evolution of a Dipole with Higher Resolution. The initial surfaces $dx \cdot M = 0$ are shown for the initial velicity field with $h = 0.025$. Only half of the surfaces are shown.

Figure 6. The Evolution of the Material Surfaces. The further evolution of the material surfaces is shown for the higher resolution calculation $h = 0.025$. This figure should be compared with fig (2).

Figure 7. The Evolution of the Material Surfaces. The further evolution of the material surfaces is shown for the higher resolution calculation $h = 0.025$. This figure should be compared with fig (4).

Figure 8. The Evolution of the Material Surfaces. The further evolution of the material surfaces is shown for the higher resolution calculation $h = 0.025$. The magnitude of the velicity is larger in regions where the surfaces are closer together and smaller in regions where the surfaces separate as can be seen from eq (9).

Figure 9. The Evolution of the Material Surfaces. The further evolution of the material surfaces is shown for the higher resolution calculation $h = 0.025$. We have removed the inner Lagrangian markers which were originally circularly shaped.

Figure 10. The Evolution of the Material Surfaces. The further evolution of the material surfaces is shown for the higher resolution calculation $h = 0.025$. We show only a third of the surfaces corresponding to the original discretization whereas in figs (5-9) we show half of the surfaces.

Figure 11. The Evolution of a Vortex Ring of Constant Vorticity. The vortex tube corresponding to a small radius of 0.2 is shown in a vortex ring of radius 0.4.

Figure 12. Deformation of a Vortex Ring. The highly deformed stage of a vortex tube is shown after it has evolved from an initially toroidal shape.

Figure 13. An Initially Swirling Flow. The initial shape of a vortex line is shown in a swirling flow.

Figure 14. The Evolution of a Swirling Flow. The evolved state of the vortex line shown in fig (13) is shown at a later time.

Figure 15. A Swirling Flow of Variable Radius. The initial shape of a vortex line in a swirling flow of variable radius is shown.

Figure 16. The Evolution of Swirling Vortex Line. The vortex line is shown which has evolved from the one shown in fig (15).

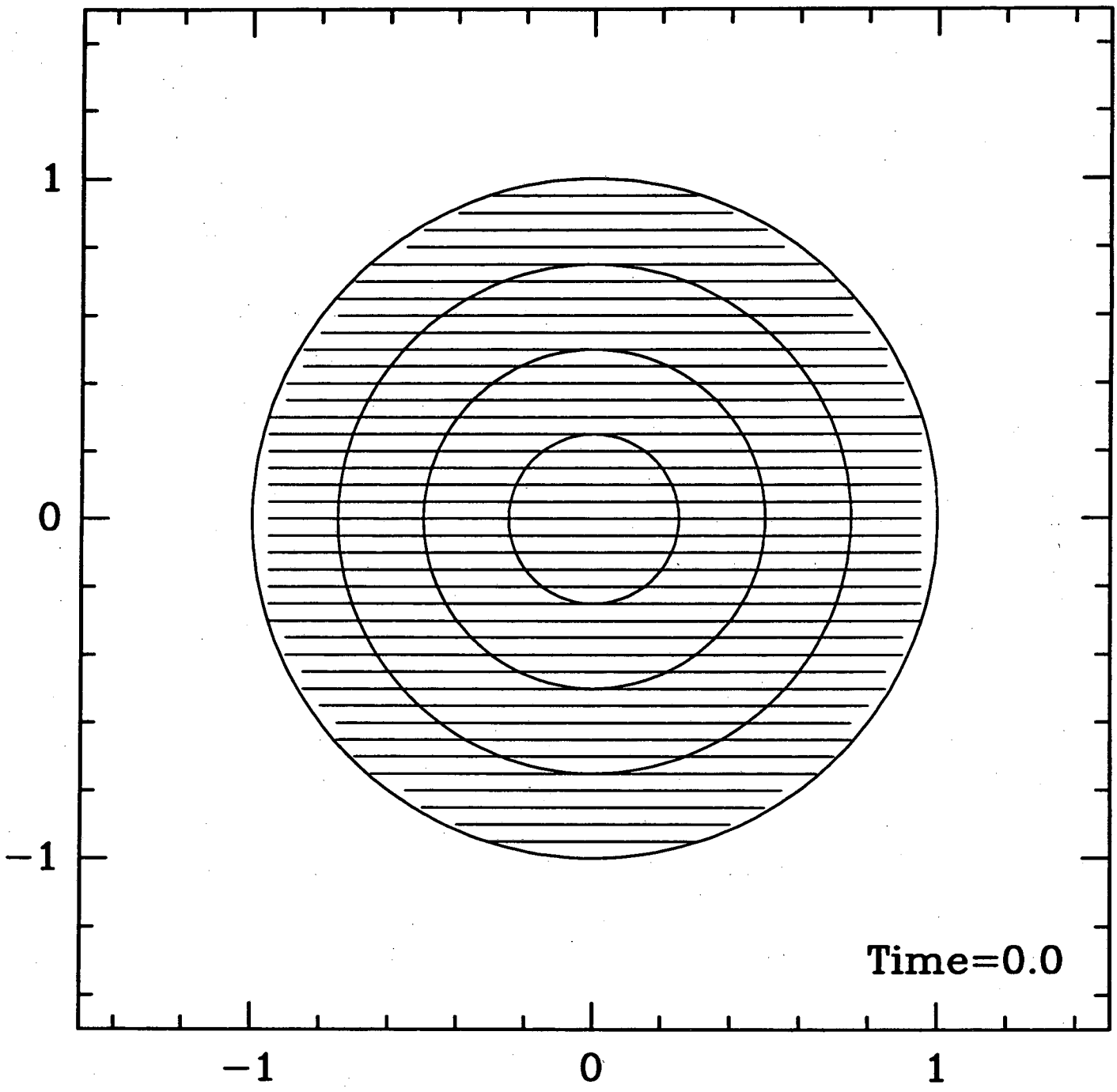

Figure 1

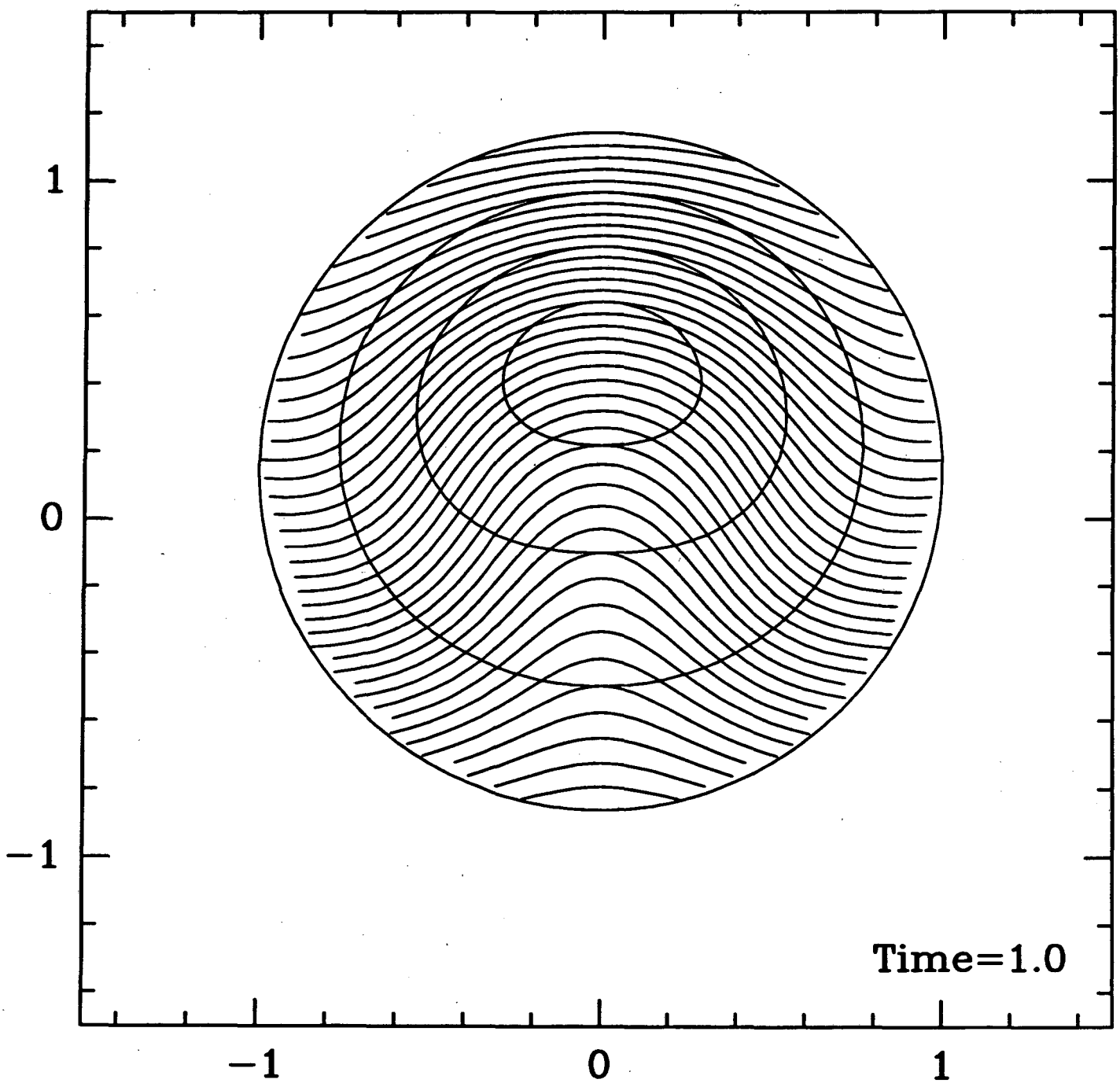

Figure 2

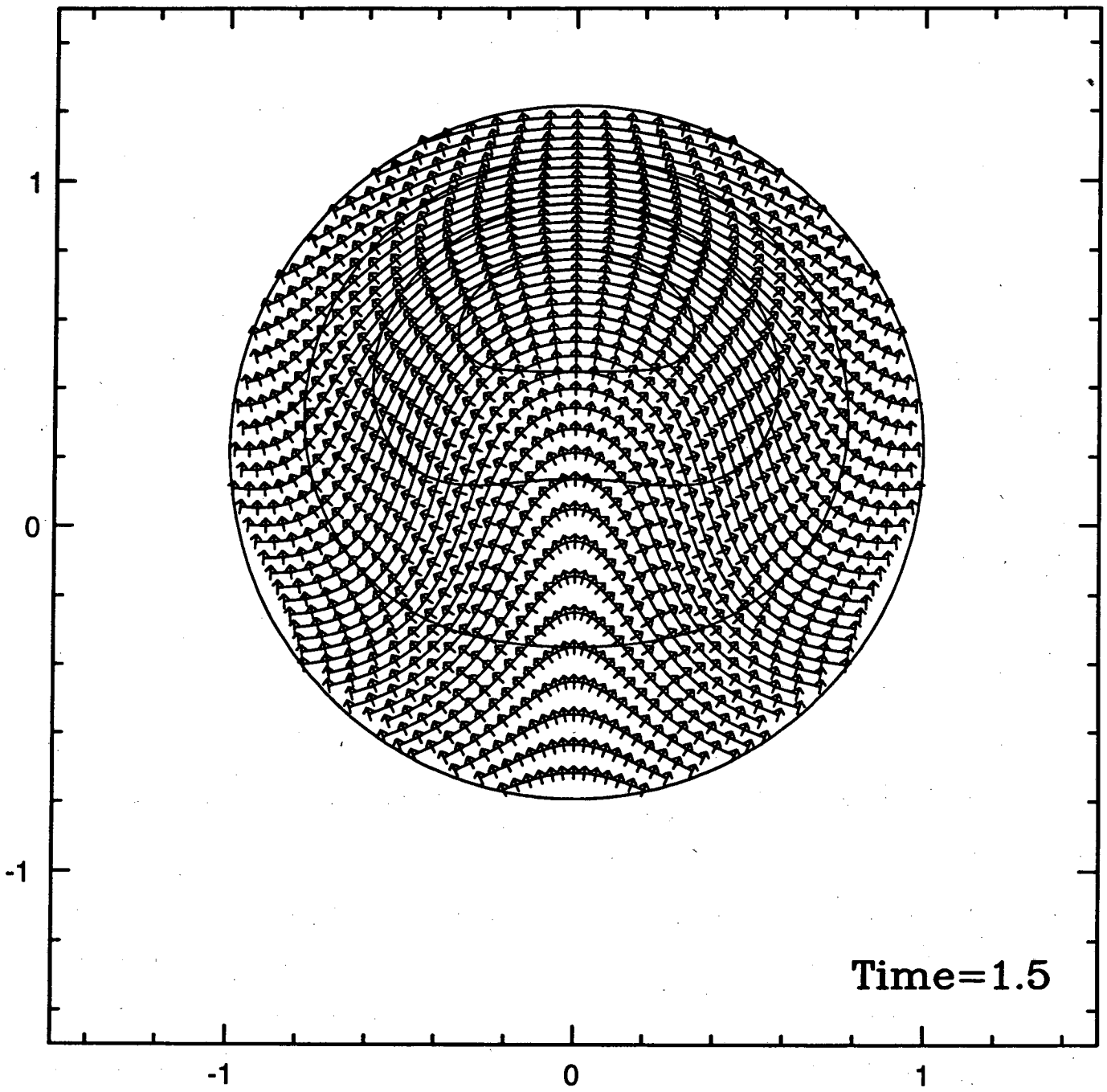

Figure 3

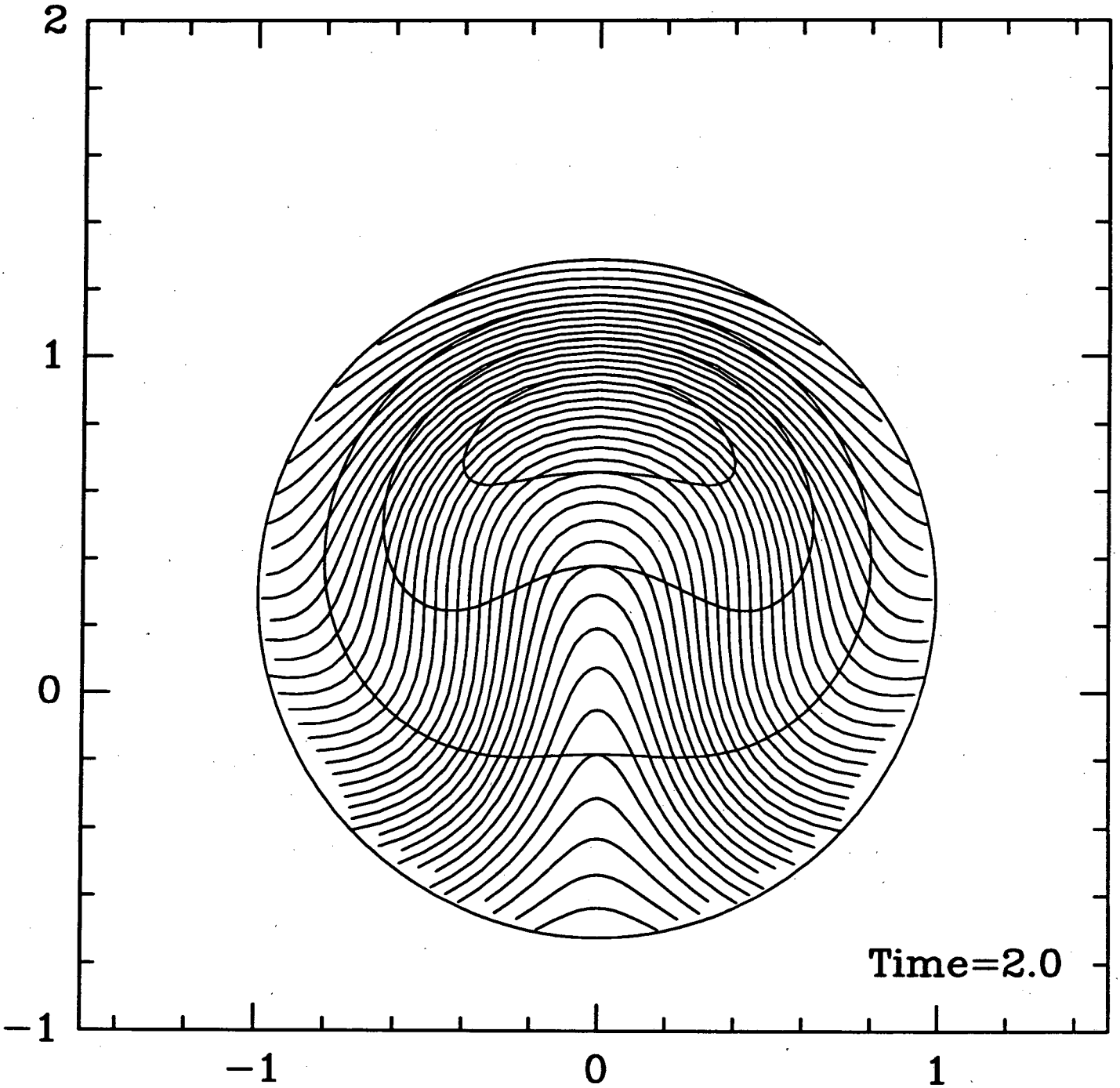

Figure 4

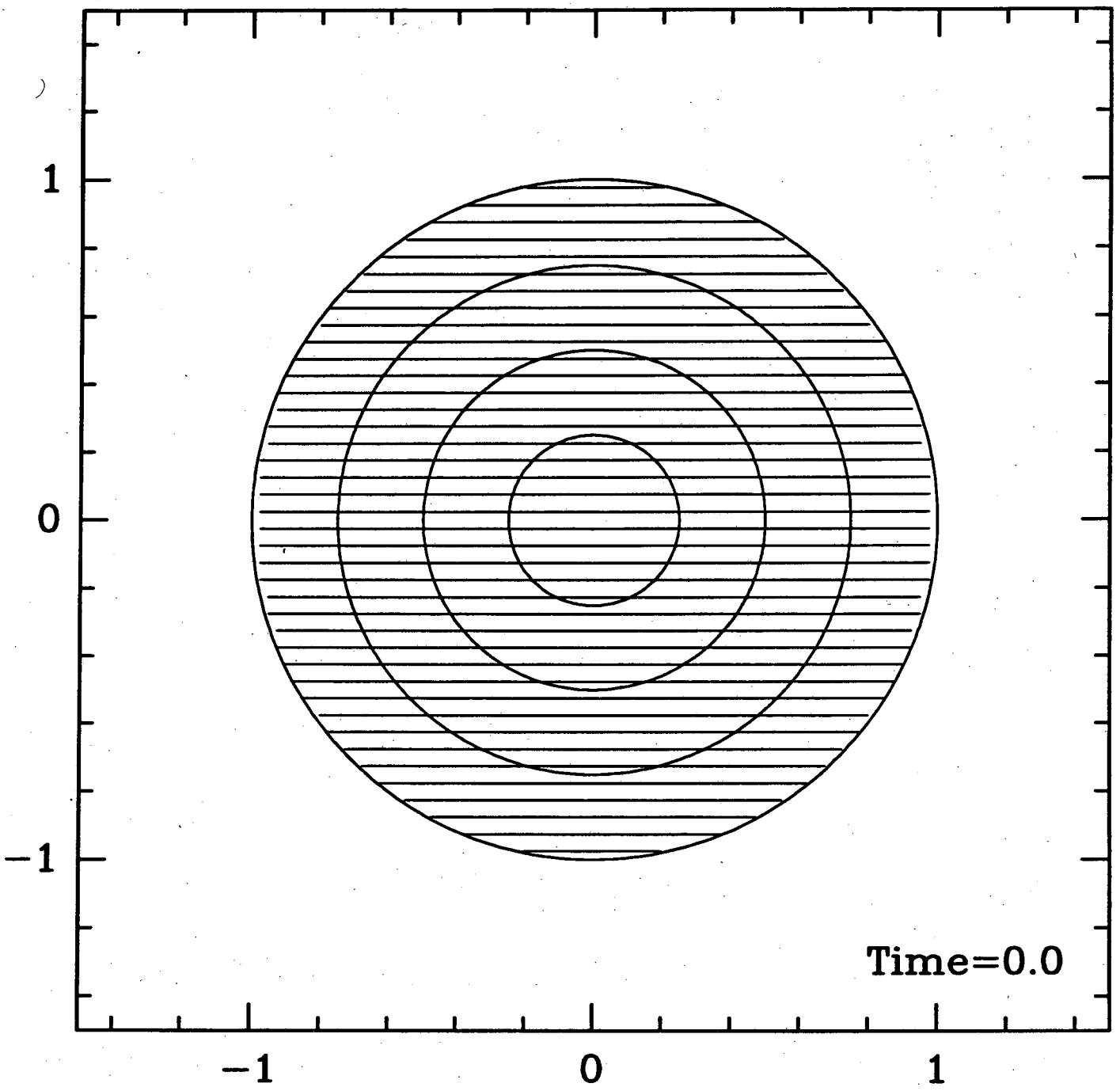

Figure 5

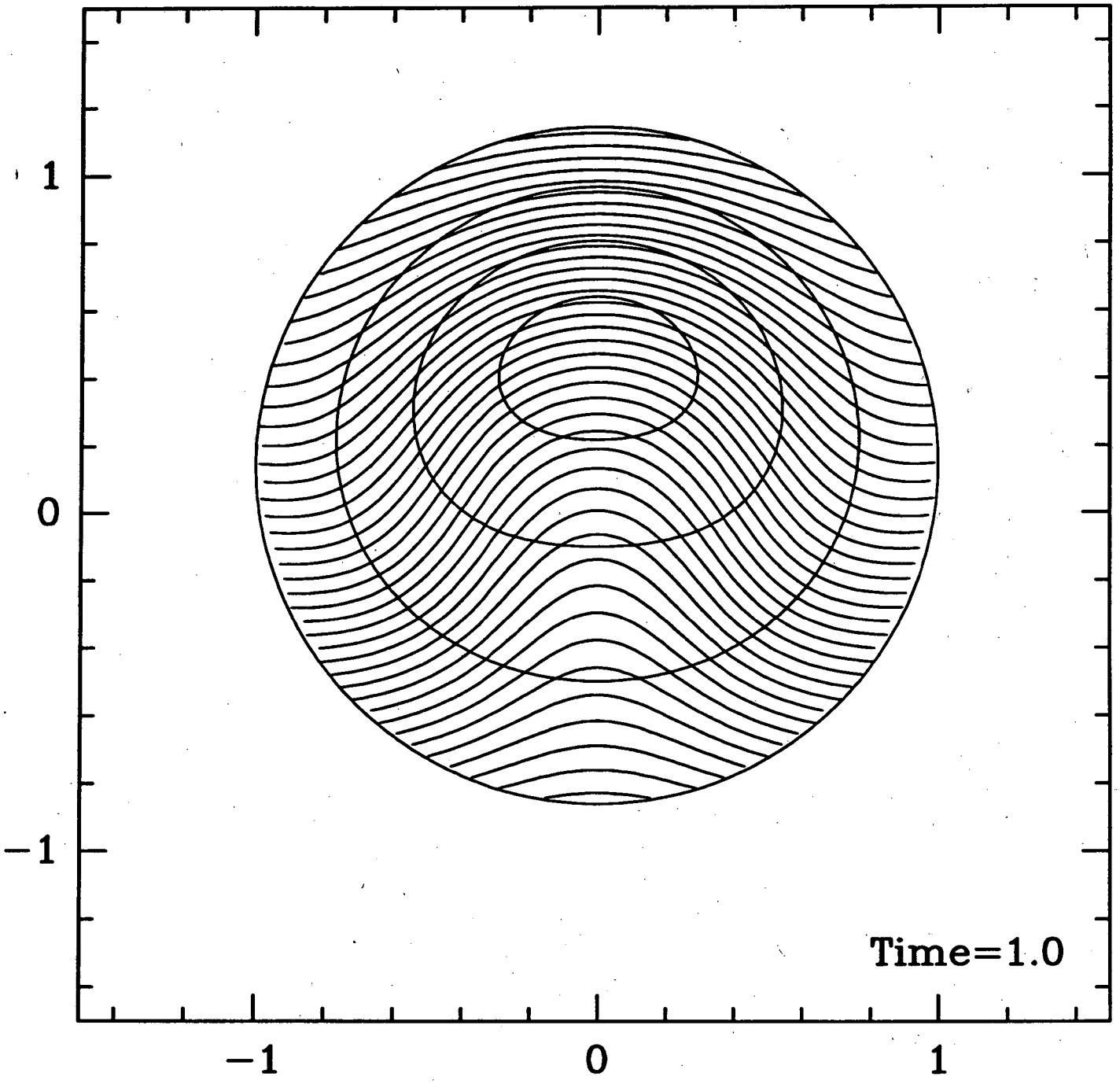

Figure 6

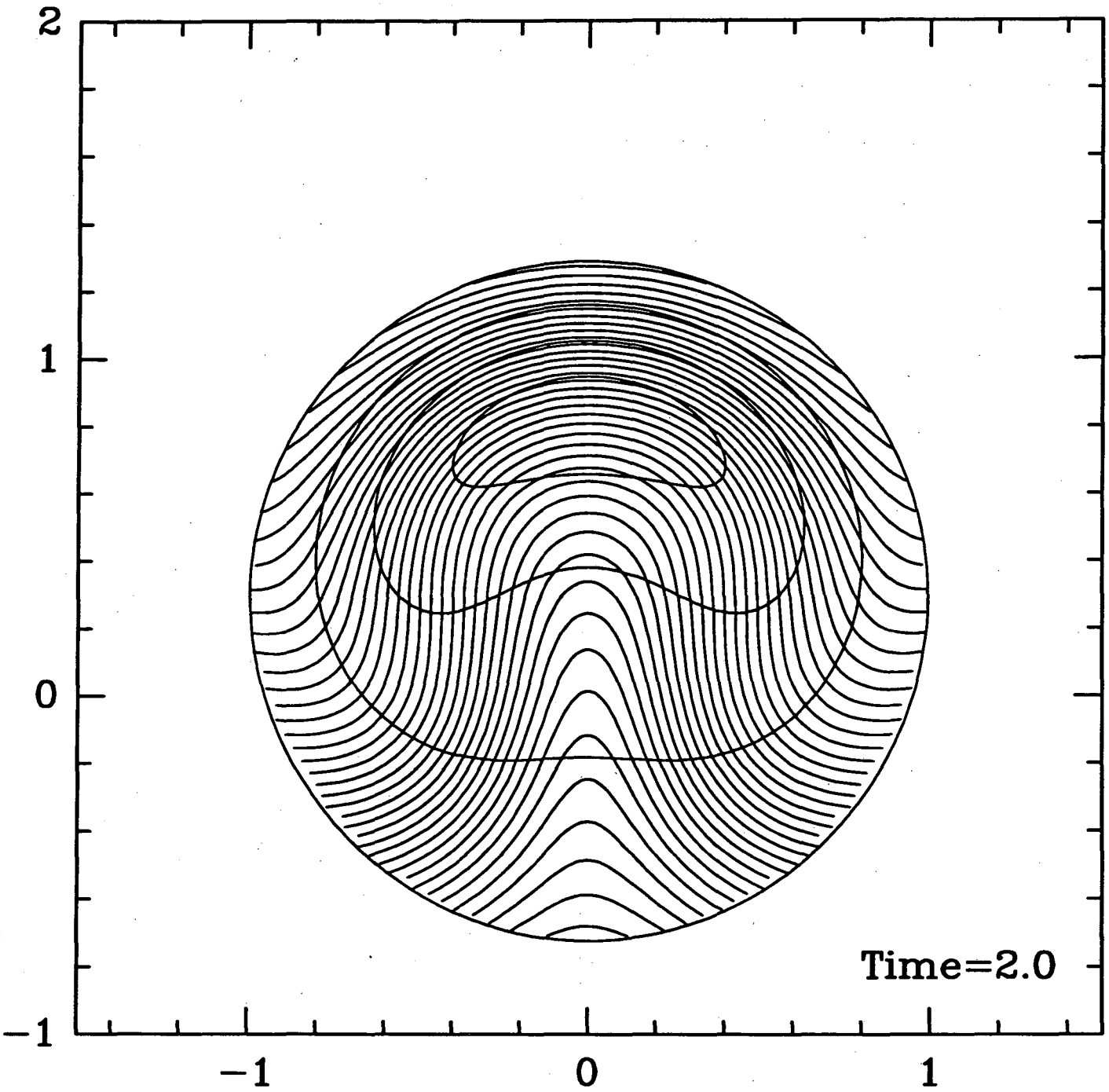

Figure 7

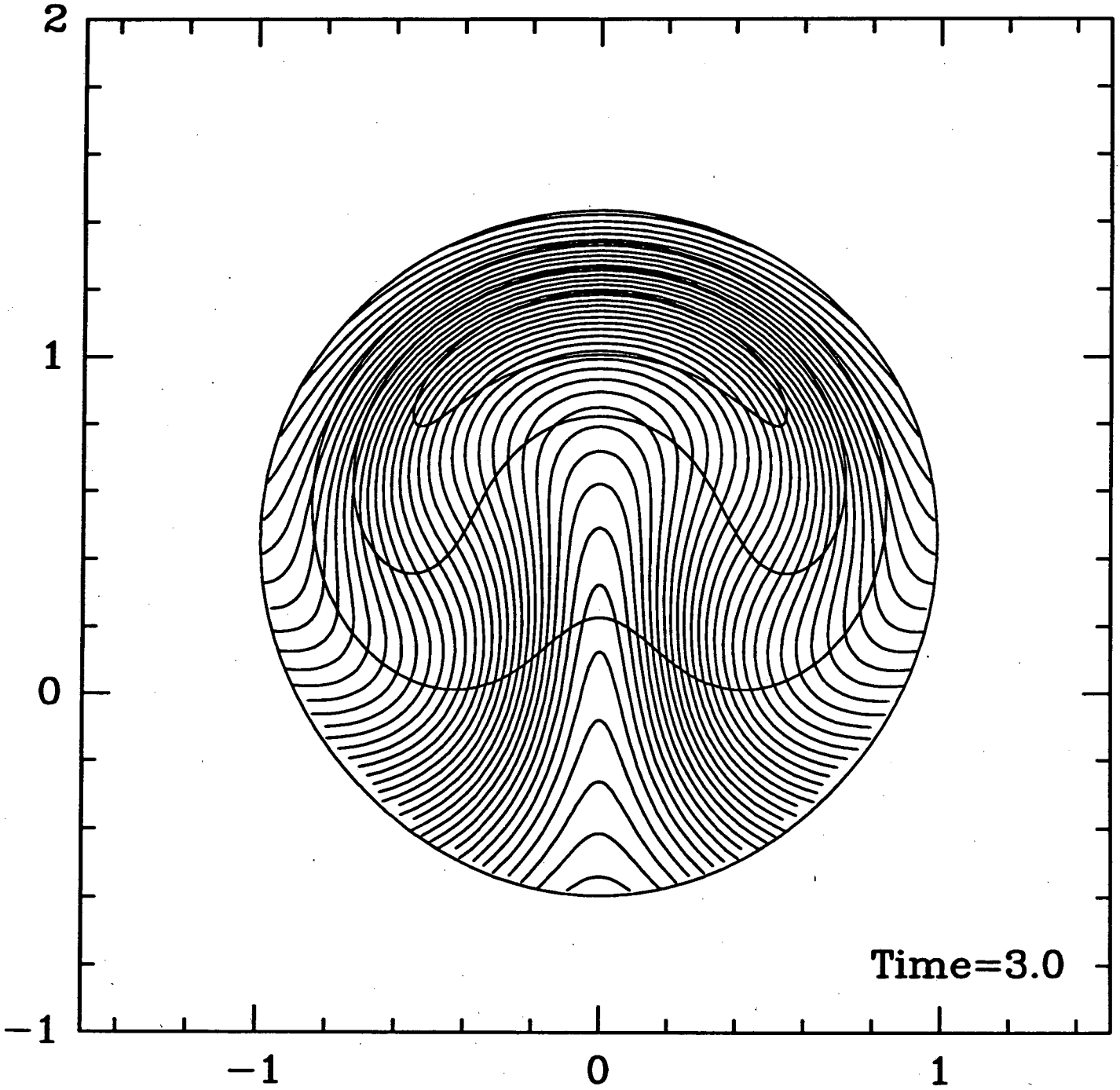

Figure 8

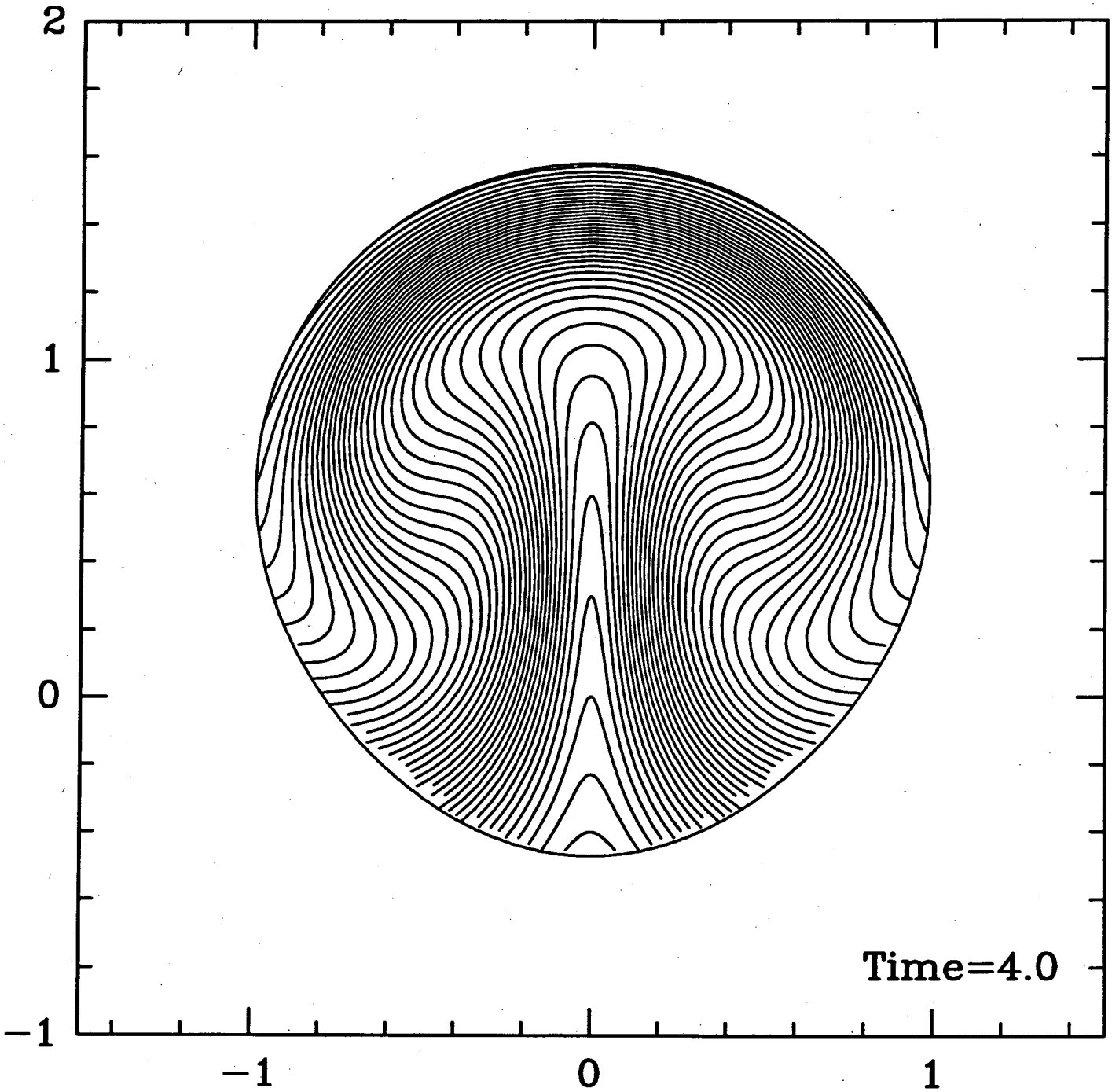

Figure 9

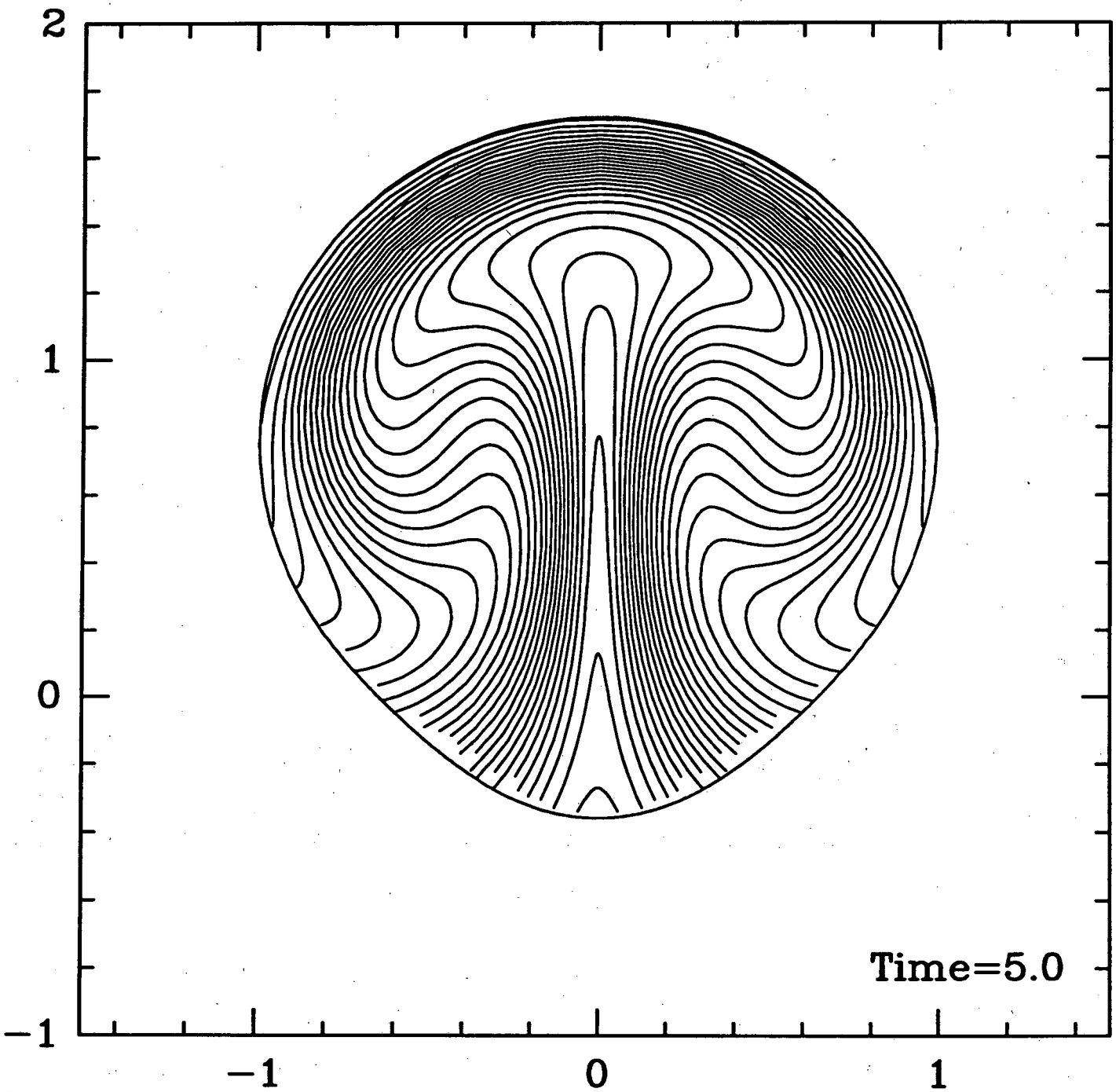

Figure 10

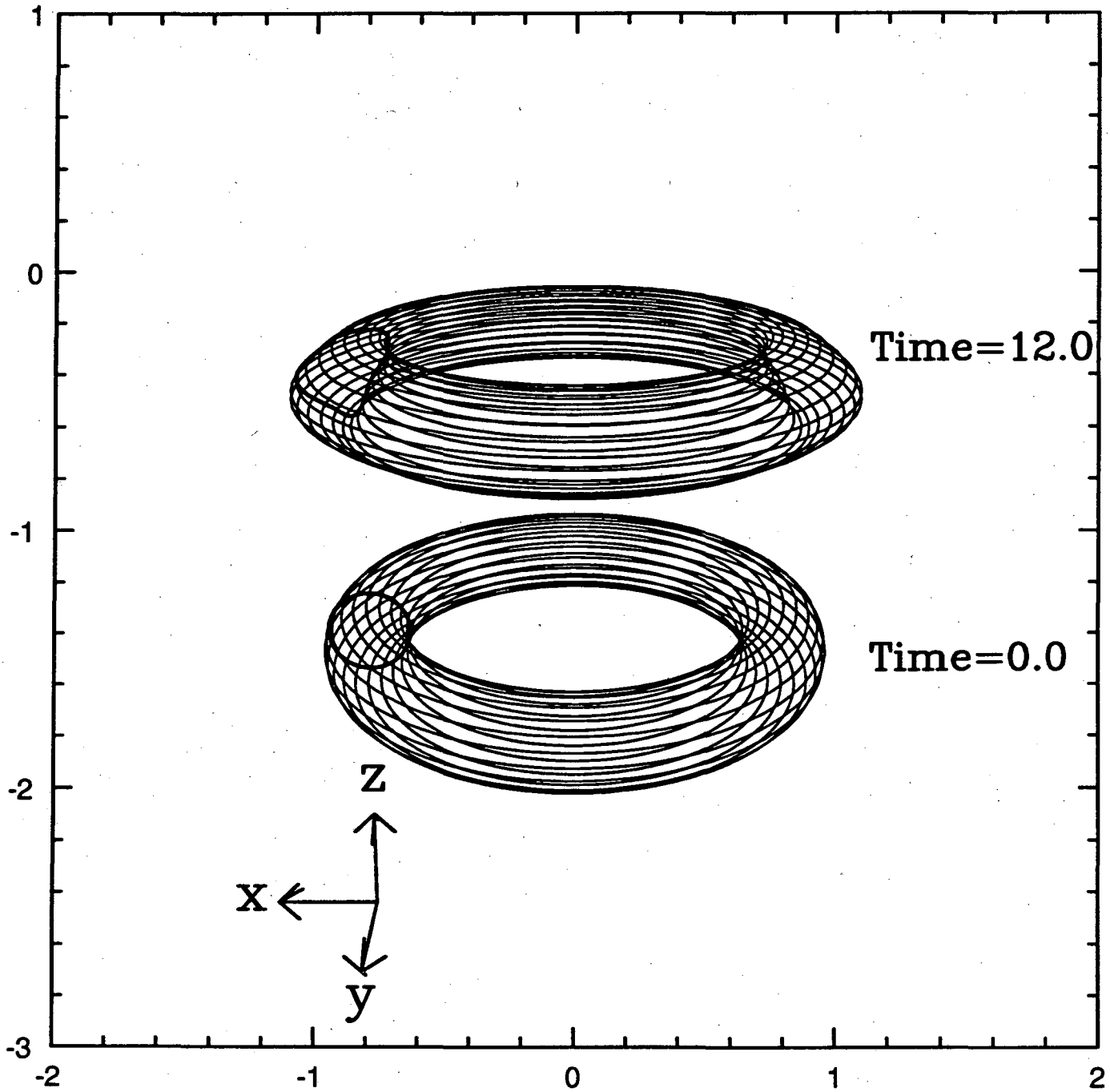

Figure 11

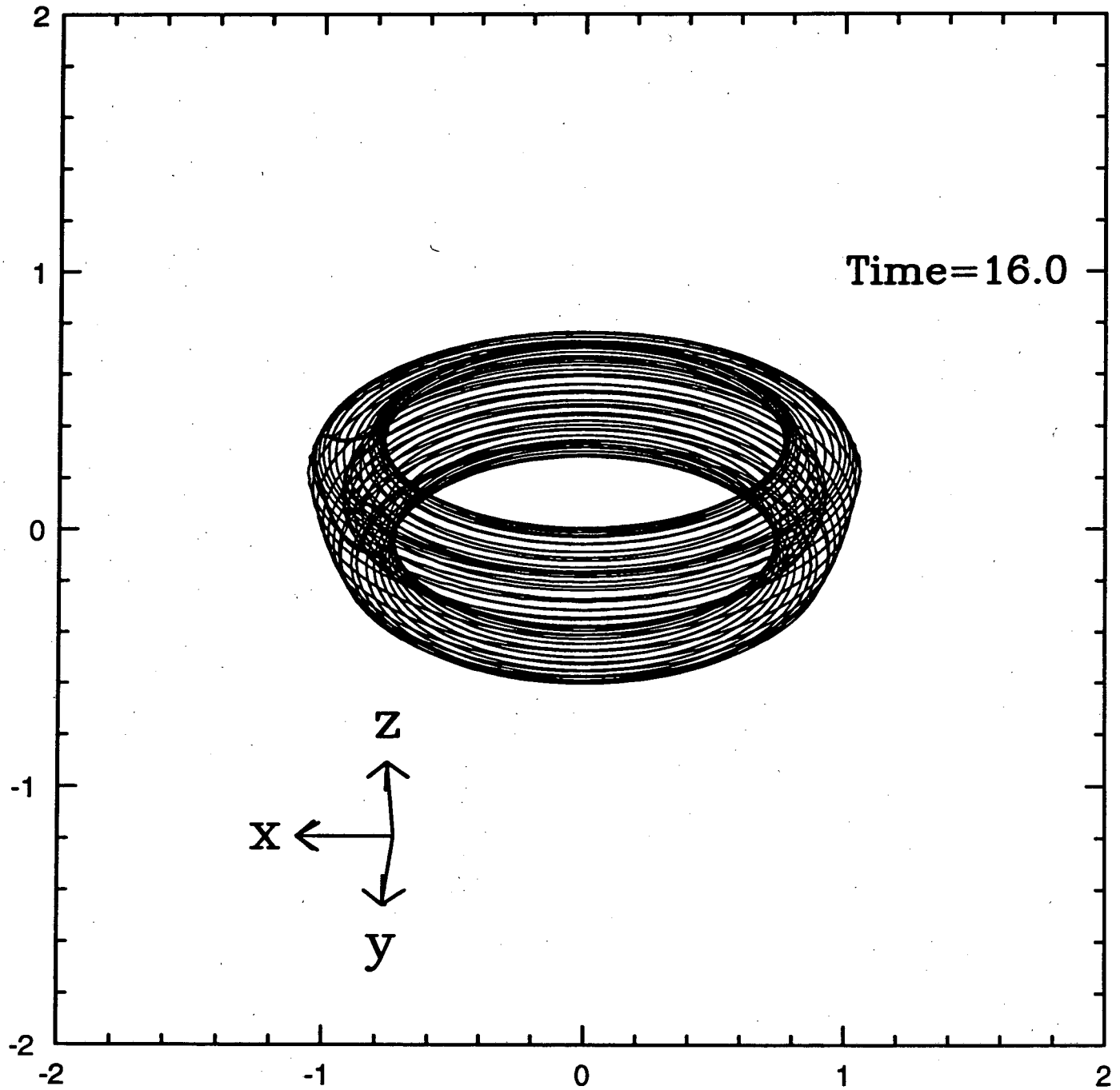

Figure 12

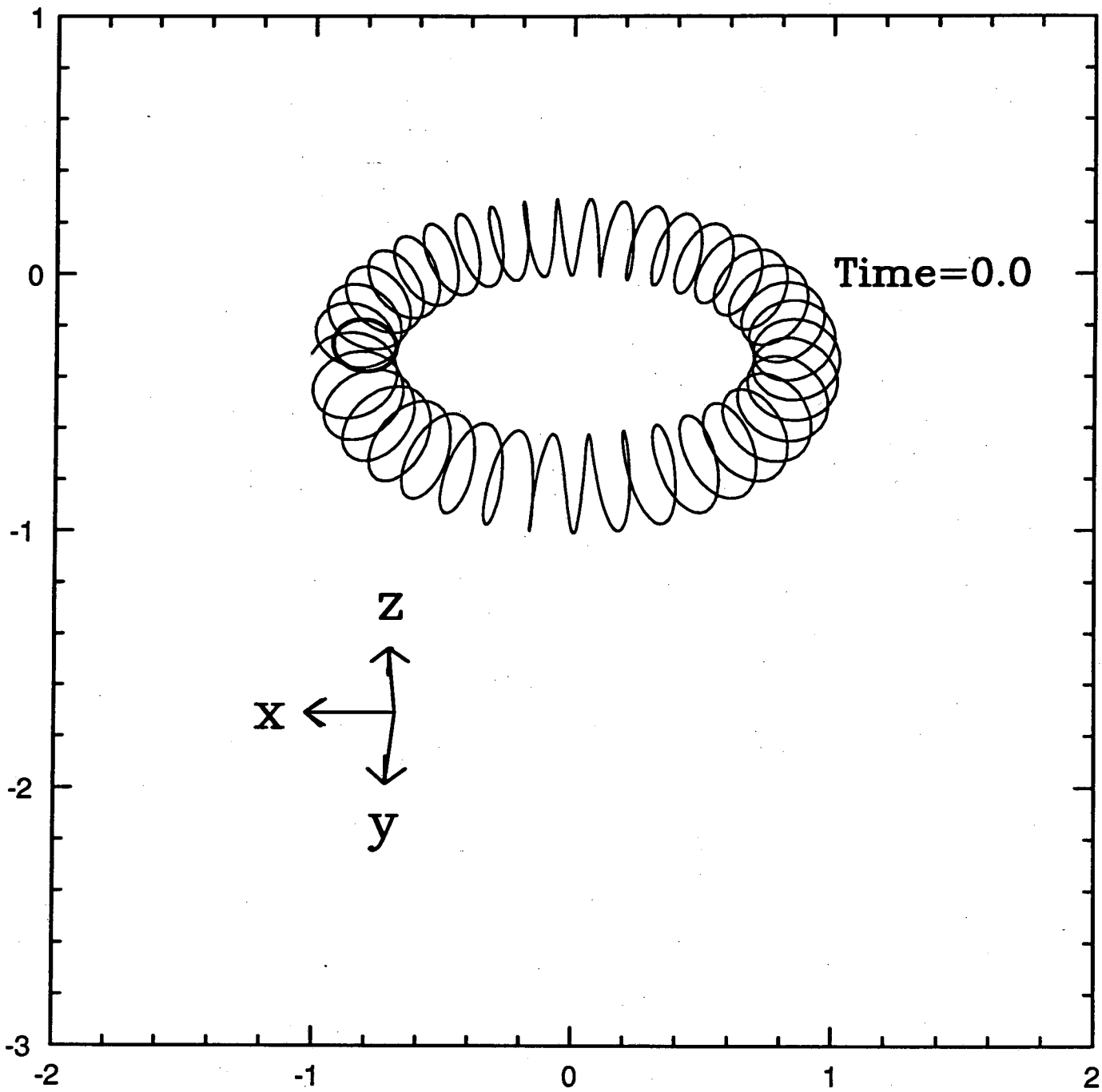

Figure 13

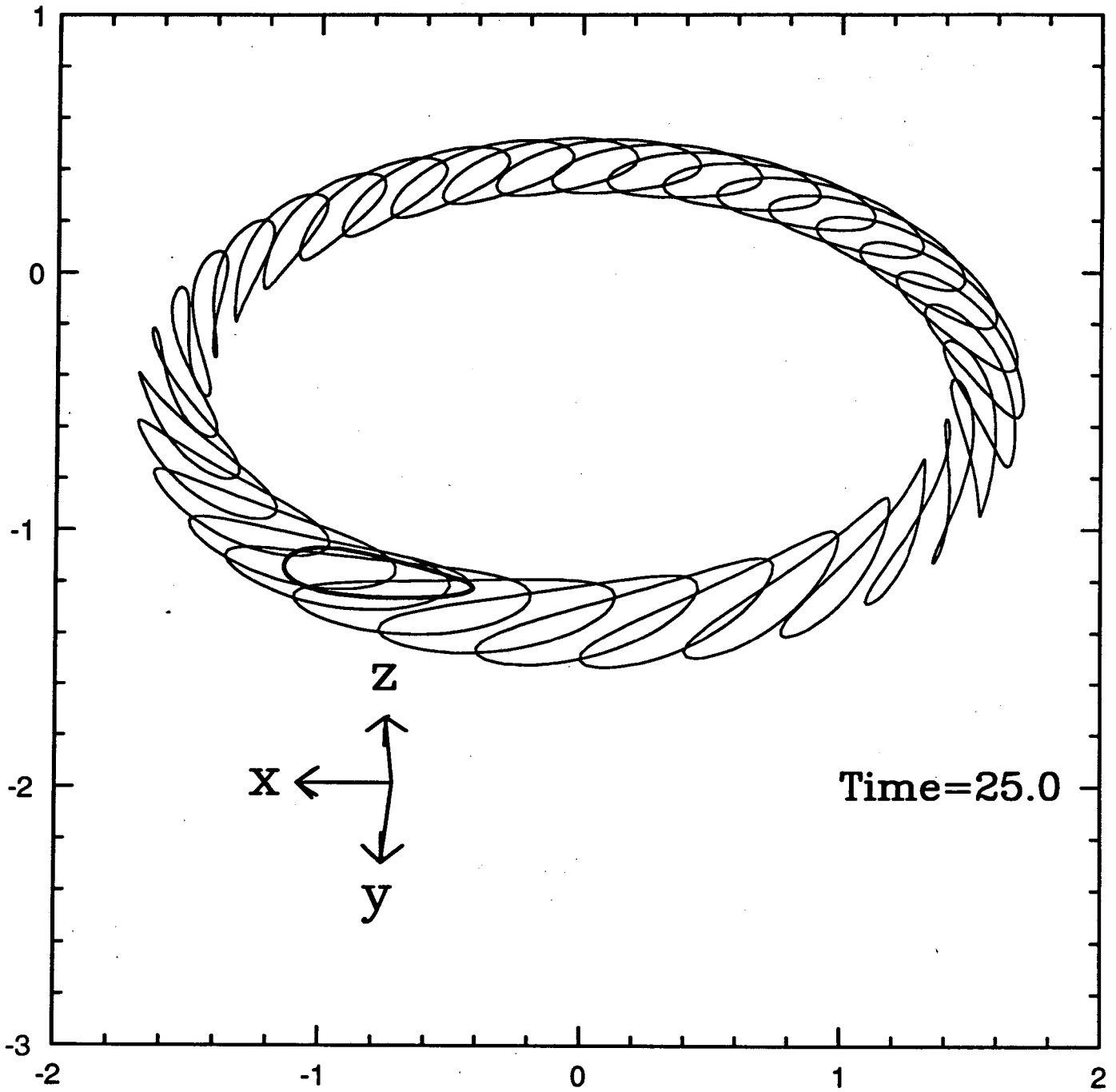

Figure 14

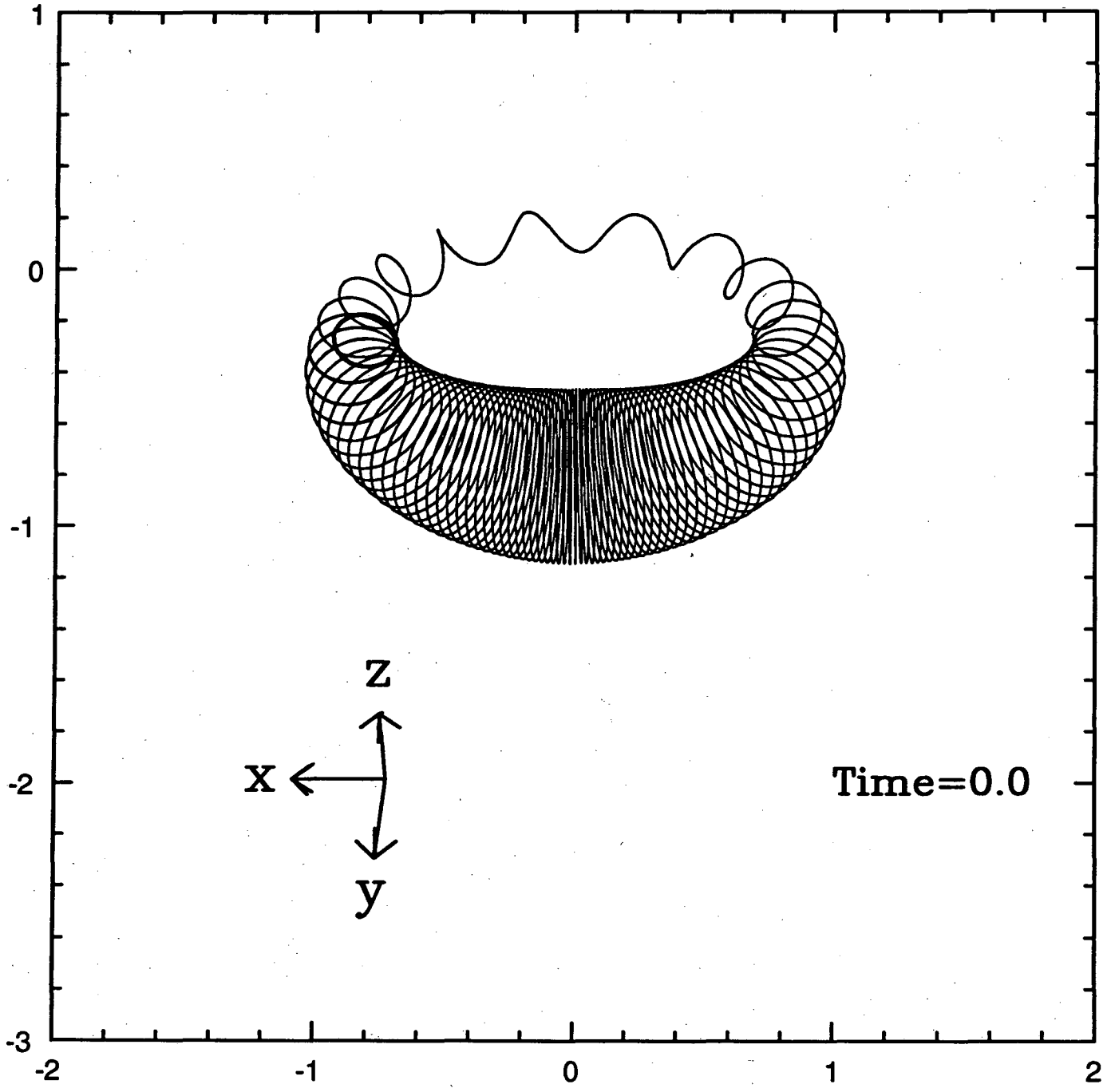

Figure 15

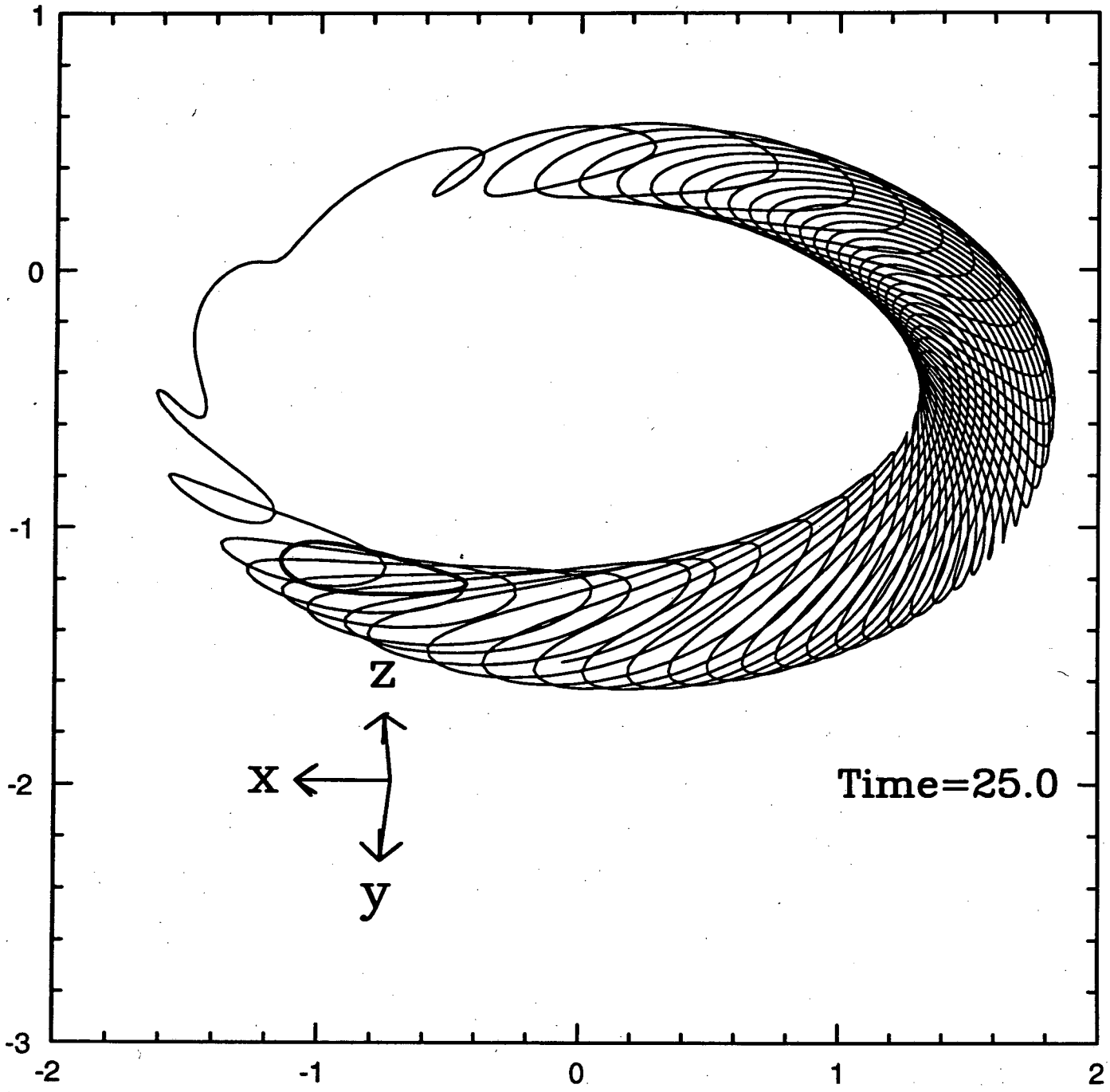

Figure 16

LAWRENCE BERKELEY LABORATORY
UNIVERSITY OF CALIFORNIA
TECHNICAL INFORMATION DEPARTMENT
BERKELEY, CALIFORNIA 94720